Received: 27 November 2024 | Revised: 03 January 2025 | Accepted: 11 January 2025

https://doi.org/10.56946/jce.v4i1.551

Journal of Chemistry and Environment

Research Article

Fabrication and Analysis of $BaTiO_3$-Nb_2O_5 Ceramics for Advanced Energy Storage Applications

Abdur Rehman Qureshi[1], Zama Jan[1,2], Arif Ullah[1], Naimat Ullah Khan[3], Uzair Khan[4], Aftab Majeed[5], Muhammad Jamshed[1,2,6*]

[1]Department of Physics, Hazara University, Mansehra-21300, Khyber Pakhtunkhwa, Pakistan
[2]School of Physics, and Xi'an Key Laboratory of Sustainable Energy & Computational Materials Science, Xi'an Jiaotong University, Xi'an 710049, P. R. China.
[3]Materials Modeling and Simulation Lab, University of Science & Technology Bannu 28100, Department of Physics, Khyber Pakhtunkhwa, Pakistan.
[4]Department of Chemistry, Abdul Wali Khan University Mardan-23200 Khyber Pakhtunkhwa, Pakistan.
[5]Department of Chemistry, Islamia College Peshawar- 25120 Peshawar, Khyber-Pakhtunkhwa, Pakistan.
[6]School of Chemistry, and Xi'an Key Laboratory of Sustainable Energy Materials Chemistry, Xi'an, Jiaotong. University, Xi'an 710049, P. R. China.
*Correspondence E-mail: muhammadjamshed@stu.xjtu.edu.cn

Abstract

As the demand for high-performance energy storage systems surges, dielectric materials have emerged as frontrunners due to their exceptional power density. Yet, their relatively low energy density has long been a bottleneck for practical deployment. This study breaks new ground by addressing this limitation, focusing on the enhancement of Barium Titanate-based ceramics for energy storage through the strategic incorporation of Niobium Oxide (Nb_2O_5). By investigating the effects of Nb_2O_5 on 0.98BT-0.02BMC ceramics, we unlock unprecedented improvements in both dielectric and energy storage properties. X-ray diffraction (XRD) analysis reveals the stability of a single perovskite phase across all compositions, paving the way for reliable performance. Most strikingly, the x = 4 composition delivers a groundbreaking dielectric constant (~2200) alongside a remarkable energy density of 1.40 J/cm^3 and a recoverable energy density of 1.10 J/cm^3, achieving an efficiency of 78.8%. These extraordinary results propel the material to the forefront of next-generation energy storage technologies, making it a powerhouse for high-demand applications such as power pulse systems. With its unparalleled combination of high energy density, exceptional efficiency, and long-term stability, this material holds the promise to redefine energy storage solutions, setting new benchmarks in both performance and reliability.

Keywords: Dielectric materials, Barium Titanate-Niobium Oxide, Energy storage application.

1. Introduction

Materials science explores how the properties of solid materials are shaped by their composition and structure, providing insights into their behavior and potential applications [1]. Energy is essential for all forms of life and for performing any meaningful work in the universe. Without energy, life cannot exist [2]. Recognizing the critical role of energy, scientists are dedicated to discovering new resources and improving the capacity and efficiency of existing energy sources [3]. Currently, scientists around the world are working to improve and expand the capacity for renewable energy production. According to literature, by 2019, the global renewable energy production capacity reached 2536 GW, with contributions from breeze energy 622 GW, sun energy 585 GW, bioenergy 125 GW, geothermic energy 14 GW, and ocean energy 500 MW [4]. Renewable energy, despite its growing importance, is not consistently available, which creates a significant challenge in ensuring a reliable and continuous supply [5].

To address this issue, there is an increasing demand for energy storage systems [6]. These systems are primarily classified into two categories: long-term and short-term, based on the duration for which energy is stored [7]. This classification helps meet the varying needs of different applications, providing effective solutions to manage the intermittent nature of renewable energy sources [8]. Among the various long-term energy storage systems, batteries stand out as one of the most intriguing and promising solutions [9]. The market offers two main types of batteries, one is primary and the other is secondary. Primary batteries, which are non-rechargeable, are known for being lightweight and affordable. The more common kinds of primary batteries include zinc-carbon, alkaline, mercury oxide, lithium (Li), silver oxide, and zinc-air batteries [10, 11]. Secondary batteries, which can be recharged and hold a significant amount of energy, offer a more sustainable solution for energy storage. Among the most popular types are lithium-ion (Li-ion), nickel-metal hydride (NiMH), nickel-cadmium (NiCd), and lead-acid batteries, each contributing to advancements in energy storage technology [12, 13].

Batteries generally offer a high energy storage density, ranging from 10 Wh/kg to 300 Wh/kg [14]. However, the movement of charged particles within the battery tends to be slow, which limits its power density to around 500 W/kg [15]. Capacitors are typically utilized for short-term energy storage due to their ability to deliver rapid bursts of power. These devices can be classified into polar and non-polar types, as well as fixed and variable configurations, depending on their design and application. While capacitors excel in providing very high-power densities, ranging from 10^1 to 10^8 W/kg, their energy storage density is comparatively low. Most capacitors store less than 30 Wh/kg of energy, making them ideal for applications where quick energy release is required, but not for long-duration energy storage [16]. A dielectric material is an electrical insulator that experiences polarization when exposed to an external electric field. This polarization occurs as the material's molecular dipoles align with the field, influencing its electrical properties [17]. High energy density (HED) capacitors, particularly those based on dielectric materials, are essential for a range of applications, including military technologies like electric armor, medical devices such as X-ray machines, and power storage modules. This has led to extensive research in both academic and industrial sectors focused on creating smaller, lighter, and more affordable HED capacitors [18]. High energy density capacitors must exhibit rapid charge-discharge response, excellent temperature stability, high breakdown strength, and high-power density. For certain specialized applications, these capacitors are also required to operate at temperatures of up to 250°C.

Dielectric materials must be carefully selected to meet these stringent requirements. Here is an overview of the materials that are considered promising or commonly used for high energy density capacitor's applications [19]. Ceramic dielectrics are preferred over polymer dielectrics for energy storage applications due to their high dielectric constants, low energy loss, quick charge-discharge response, and ability to withstand higher operating temperatures for extended periods [20]. In ceramics, a trade-off often exists between dielectric constant and breakdown strength. Glass ceramics are created by embedding nano-crystallites in a glass matrix and heating them at particular temperatures. The crystalline phase within the glass ceramics can result in a dielectric constant that exceeds the permittivity of the original glass matrix. The $BaTiO_3$-Nb_2O_3 sample, processed under optimal conditions, demonstrates a dielectric constant ranging from 650 to 850 at a frequency of 1 kHz, along with a low tangent loss of approximately 0.02 over a temperature range of 25-150°C, highlighting its promising potential for energy storage applications [21]. These remarkable properties make it an excellent candidate for further research and development in advanced dielectric materials for high-performance energy storage systems [8, 22].

2. Materials and methods

The solid-state reaction route is an effective technique for manufacturing ceramics, involving key steps such as selecting and mixing raw materials, heating at high temperatures to

initiate chemical reactions, and forming a homogeneous ceramic phase. Subsequent processes like grinding, sintering, and shaping ensure the final material possesses desirable properties, including mechanical strength, thermal stability, and electrical performance.

2.1. Raw materials and characterization techniques

In this study, the appropriate raw materials for preparing Nb_2O_3 doped $0.96BaTiO_30.04Bi(Mg_{0.5}Ce_{0.5})O_3$ ceramics were selected based on literature recommendations. Highly pure raw materials, including MgO, TiO_2, $BaCO_3$, Nb_2O_3, Bi_2O_3, and CeO_2, were carefully weighed in stoichiometric ratios and mixed together. The chemicals used MgO (>99%), TiO_2 (>99%), $BaCO_3$ (>99.5%), $BaCO_3$ (>99.5%), Nb_2O_3 (>99.9%), and CeO_2 (>99.5%) were sourced from Sigma-Aldrich. For crystal structure and phase analysis, X-ray diffraction (XRD) was conducted using a JDX 3532 Jeol XRD system, while scanning electron microscopy (SEM) on a Hitachi SU5000 was employed to examine the grain size and nature of the synthesized materials. The dielectric constant and tangent loss of the samples were measured across a frequency range of 1 kHz to 1 MHz and a temperature range of 30˚C to 500˚C using a computer-interfaced L.C.R meter (E4980A, Agilent, U.S.A).

2.2. Stoichiometric ratios and solutions

A significant portion after selecting the raw materials is ensuring precise stoichiometric ratios, as even slight deviations can significantly impact the desired outcome. Isopropanol is utilized as a binder, and zirconia balls are employed as grinding media to achieve the appropriate particle size. The mixture is then dried in an oven at 95˚C for 24 hours to yield uniform powders [23]. The following stage involves blending the raw materials using a ball milling machine, a critical process that influences the dielectric characteristics of the solid solution. In this research, to prepare $0.96BaTiO_30.04Bi(Mg_{0.5}Ce_{0.5})O_3$, the compounds MgO, TiO_2, $BaCO_3$, Nb_2O_3, Bi_2O_3, and CeO_2 were precisely measured and combined in the correct stoichiometric proportions [24].

2.3. Calcinations, Grinding and Pellets Formation

The precursor mixtures were subjected to ball milling for 24 hours, utilizing ZrO_2 balls as grinding media and isopropanol as a lubricant to facilitate the formation of fine, homogeneous slurries with optimal flow properties. Following this, the slurries were transferred to a furnace for subsequent thermal processing. In the present study, the milled powders were first dried at 95°C to remove excess moisture, followed by calcination at 850°C for 2 hours to induce phase transformation and promote solid-state reactions. After the Nb_2O_3 doped $0.96BaTiO_30.04Bi(Mg_{0.5}Ce_{0.5})O_3$ powder underwent a second round of milling under identical conditions, with isopropanol as a lubricant and zirconia balls as grinding media. The powders were again dried at 95˚C for 24 hours to achieve a uniform consistency. Subsequently, the powder was crushed and mixed with aqueous polyvinyl alcohol (PVA) as a binder to enhance the palletization process. The well-calcined powders, comprising Nb_2O_5 (X = 2, 4%) and $0.96BaTiO_30.04Bi(Mg_{0.5}Ce_{0.5})O_3$, were compacted into cylindrical pellets with dimensions of 1mm in height and 12mm in diameter using a hydraulic press at 100 MPa. Finally, the pellets were subjected to a thermal treatment at 600˚C for 2 hours to effectively remove the PVA binder and facilitate the sintering process.

3. Results and discussion

3.1. Phase Examination

Figure 1 displays the X-ray diffraction (XRD) patterns of the $0.96BaTiO_30.04Bi(Mg_{0.5}Ce_{0.5})O_3$ + x wt% Nb_2O_3 (x = 0, 2, 4) samples. For the x = 0 composition, a single perovskite phase is observed, with the high-resolution XRD pattern around 2θ = 45° showing peak splitting between the (002) and (200) reflections.

This splitting corresponds to card # 70-4760 and indicates a tetragonal structure, which is consistent with previous reports for $BaTiO_3$-based ceramics. As the Nb_2O_3content increases to 2 wt% and beyond, the split peaks merge, suggesting the formation of a pseudo-cubic phase. Notably, no secondary phases were identified in any of the compositions analyzed in this study.

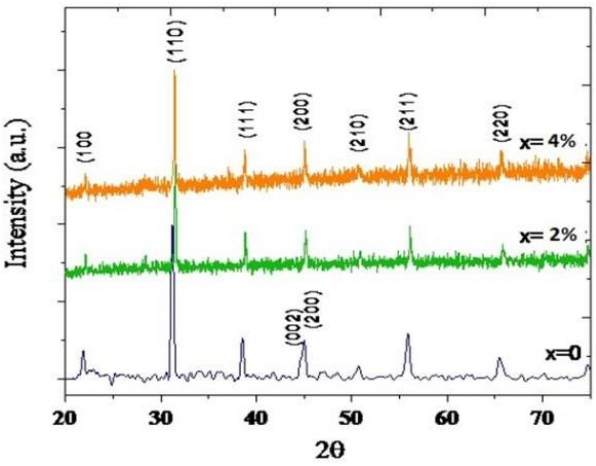

Figure 1. XRD patterns of (0.98BT– 0.02BMC+xwt%Nb_2O_5, x=0, 2, 4) ceramics.

3.2. Microstructure examination

The SEM images of the etched surfaces of $0.96BaTiO_3 0.04Bi(Mg_{0.5}Ce_{0.5})O_3$ + x wt% Nb_2O_3 (x = 2, 4) ceramics show clear micro-structural differences in finger 2 (a, b, and c), respectively. The x=2 composition exhibits a porous microstructure, indicating incomplete sintering, which may reduce charge storage capacity and efficiency due to the high porosity that can hinder electron movement. On the other hand, the x = 4 composition has a denser microstructure, improving the material's dielectric properties, mechanical strength, and thermal stability. The larger grain size (greater than 1 µm) in x = 2 composition could create more grain boundary sites that reduce dielectric strength, while the smaller grain size (less than 1 µm) in x = 4 composition, enhances the material's ability to handle higher electric fields and improves energy storage capability.

3.3. Measurement of dielectric properties

The understudy compositions' dielectric characteristics are computed using a vector network analyzer. The following formula can be used to calculate the temperature factor T_f value over the temperature range of T_0 to T in °C.

$$T_f = \frac{f_1 - f_2}{f_1 (T - T_0)}$$

Here, T_f represents the time frequency, while f_1 and f_2 denote the frequencies at temperatures T_1 and T_2, respectively. Figure 3(a-c) illustrates the variation in dielectric constant (εr) and tangent loss (tan δ) for (0.98BT– 0.02BMC + x wt% Nb_2O_3 x = 0, 2, 4) samples over a temperature range of 25-500◦C at frequencies of 1 kHz, 10 kHz, 100 kHz, and 1 MHz. In Figure (a), the Curie temperature (T_c) for the x = 0 composition is clearly marked by a sharp transition at approximately 125°C, signifying the shift from the ferroelectric to the paraelectric phase [25]. For x = 0 at 1 kHz, the dielectric constant reaches its maximum value (εr-max) of 3400, indicating the transition from the ferroelectric to the paraelectric phase as shown in figure 3(b).

With the incorporation of 2% Nb_2O_3, the Curie temperature is shifted below room temperature shown in finger 3(b), and the maximum dielectric constants (εr-max) are measured as 670 for x = 2 and 2200 for x = 4 at 1 kHz.

The lower dielectric constant observed for the x = 2 composition can primarily be attributed to its porous microstructure, which results in a lower density compared to the x = 4 composition. The porous nature of the material can lead to a decrease in the overall polarization response, thus reducing the dielectric constant. Additionally, the addition of 2% Nb_2O_3 shifts the Curie temperature below room temperature (as shown in Figure 3(b)), which also contributes to the observed changes in dielectric behavior. Regarding the reduction in dielectric constant for x = 2, it is important to note that the Nb_2O_3 component itself has an inherently lower dielectric constant compared to the base material (x = 0). This addition, while reducing the dielectric constant, also brings other beneficial effects, such as a decrease in tangent loss, indicating an improvement in energy storage efficiency. While the porous microstructure in x = 2 can indeed be a limiting factor for its energy storage performance, it is worth noting that Nb_2O_3 incorporation leads to a reduction in tangent loss, as seen in Figure 3(c).

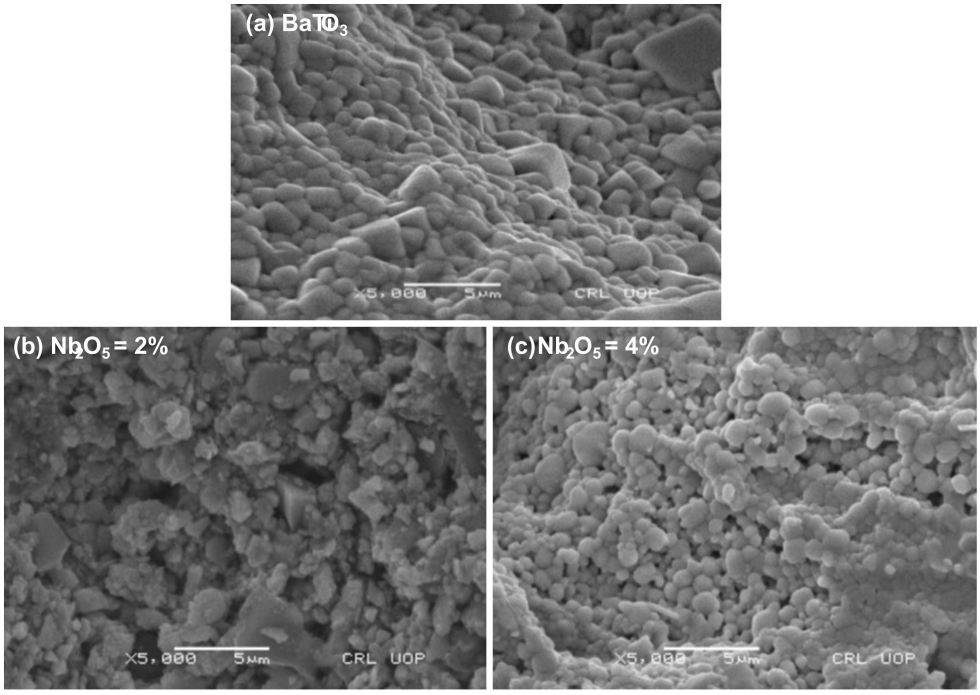

Figure 2. Scanning electron microscope image of: (a) $BaTiO_3$, (b) 0.98BT–0.02BMC+xwt%Nb_2O_5 (x=2), (c) 0.98BT–0.02BMC+xwt% Nb_2O_5 (x=4) samples.

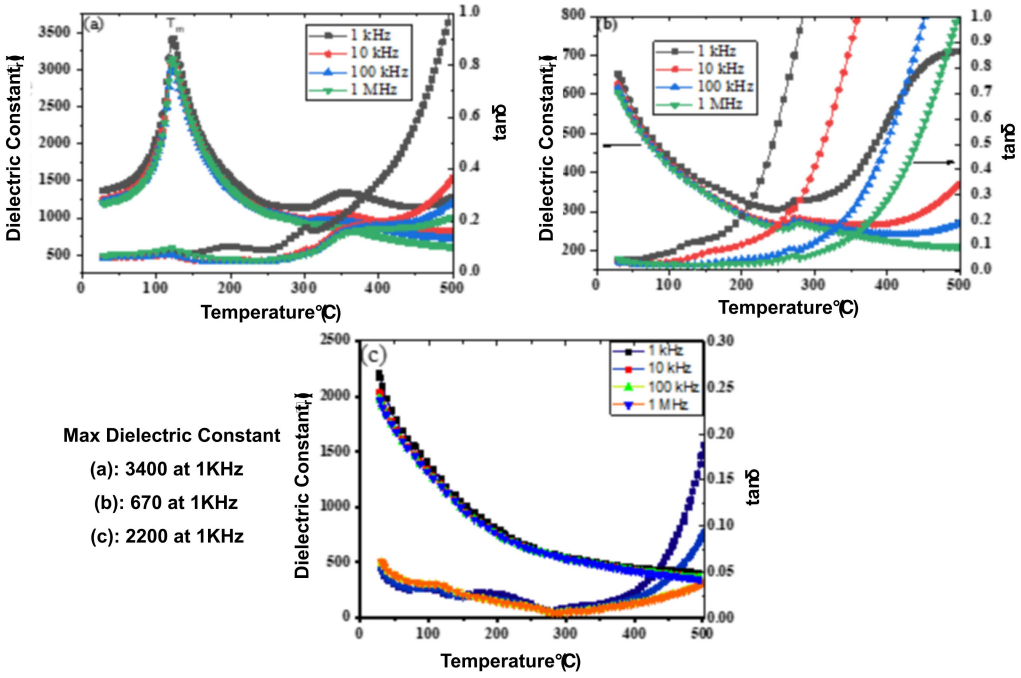

Figure 3. The variation of ε_r of (0.98BT– 0.02BMC+ xwt% Nb_2O_5 x=0, 2, 4) samples as a function of temperature at different frequencies (a) x=0, (b) x=2 and (c) x=4.

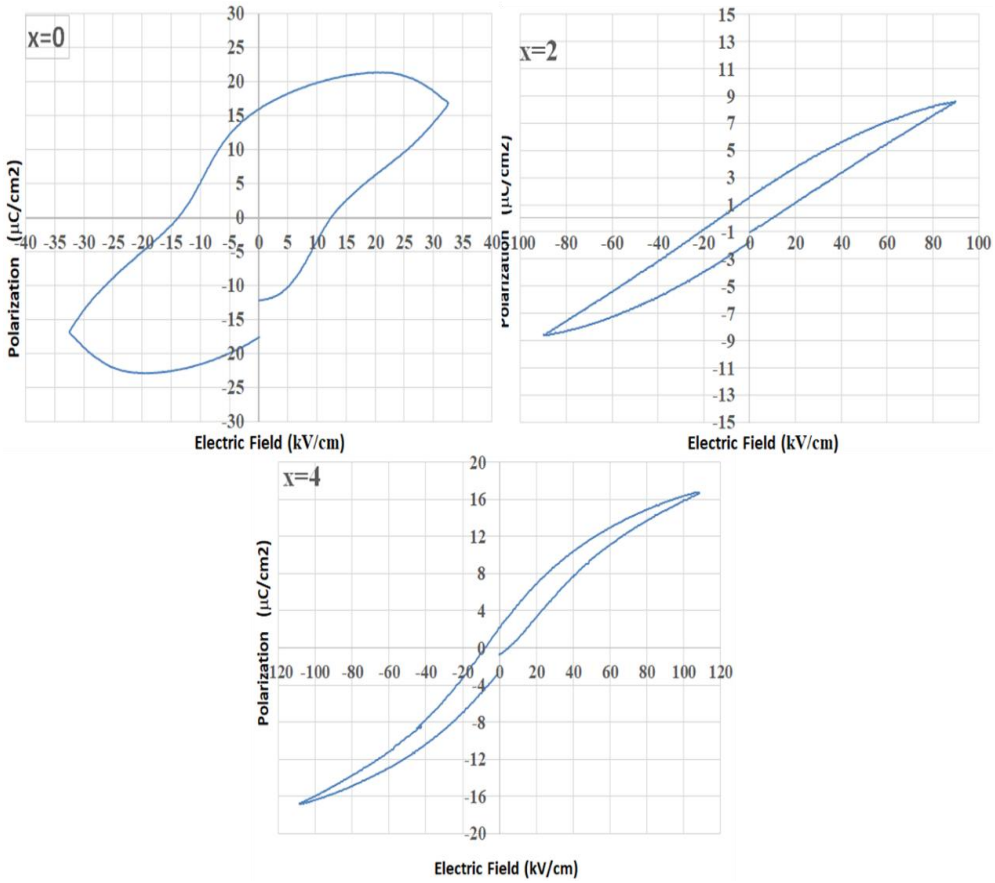

Figure 4. Polarization against Electric field Hysteresis loops of (0.98BT– 0.02BMC+xwt% Nb_2O_5 x=0, 2, 4) samples as a function of electric field.

Table 1. Polarizations, and energy storage characteristics of (0.98BT– 0.02BMC+ xwt%Nb2O5 x=0, 2, 4) samples.

Composition (x)	[P_{max}]	[P_r]	[P_{max}–P_r]	[W_{ch}]	[W_r]	[η%]
0	16.85	15.92	0.9	0.50	0.13	28
2	8.59	1.55	7.04	0.95	0.60	71
4	16.62	2.21	14.41	1.43	1.10	78

This reduction indicates enhanced efficiency, which offsets some of the potential drawbacks caused by the porosity. Moreover, the material with x = 4 (with higher Nb_2O_3 content) exhibits superior energy storage properties, including a maximal dielectric constant of ~2200, highlighting the potential for optimization in future studies. Further work could explore strategies to address the porous microstructure of x = 2 by adjusting the synthesis parameters or introducing additives to improve the material's density and structural integrity, thereby enhancing its overall performance for energy storage applications.

3.4. Analysis of P-E Loop

For the (0.98BT–0.02BMC+xwt% Nb_2O_5 x = 0, 2, 4) samples, Figure 4 displays the polarization versus electric field (P-E) hysteresis loops. With the P-E loops measured at 10 Hz for each 0.3 mm thick ceramic pellet, significant differences in the

critical or breakdown electric fields E_b and maximum polarization Pmax are seen across the samples. Energy-storage metrics including charge energy density W_{ch}, recoverable or discharge energy density W_r, and efficiency (η) are calculated using each sample's P-E hysteresis loop. Furthermore, the normal grain size and density of each sample are connected to its break-down voltage.

The P-E hysteresis loop for each composition is recorded at its respective breakdown voltage.

As shown in Figure 4, the x=0 composition displays a broad P-E loop, featuring a maximum polarization value of 16.92 C/cm^2, and a significant remnant polarization of 15.85 C/cm^2. For x=2 composition, the P-E hysteresis loop narrows, exhibiting a maximum polarization (P_{max}) of 8.59 C/cm^2 and a considerably reduced Remnant polarization of 1.55 C/cm^2 at a break-down electric field of 9 kV/cm. In a similar trend, for x=4, the material exhibits a remarkable maximum polarization of 16.82 C/cm^2, accompanied by a remnant polarization of 2.21 C/cm^2 at break-down electric field of 107 kV/cm. Thus, the higher P_{max}-P_r value in the x=4 composition significantly contributes to enhanced energy storage and recovery, making it an ideal candidate for high-density and efficient energy storage applications. The combination of elevated maximum polarization, reduced remnant polarization and a large P_{max}-P_r value in this composition offers promising potential for improving both charge and discharge energy densities.

Analysis of energy density (ADA)

The P-E hysteresis loop is used to determine the energy storage parameters for each sample, including charge energy density W_{ch}, discharge energy density W_r, and efficiency (η).

$$W_{ch} = \int_0^{P_{max}} E\,dP \quad \ldots\ldots (1)$$

$$W_r = \int_{P_r}^{P_{max}} E\,dP \quad \ldots\ldots (2)$$

The efficiency of the capacitor can be calculated using the following equation (Eq 3).

$$\eta = \frac{W_{rec}}{Ws} \times 100 \quad \ldots\ldots (3)$$

In this study, the x=4 composition achieved an impressive charge energy density (W_{ch}) of 1.40 J/cm^3, a recoverable energy density (W_{rec}) of 1.10 J/cm^3, and a remarkable efficiency (η) of 78.8%. These enhanced energy storage parameters can be attributed to the superior P_{max} and larger P_{max}-P_r differences, which set x=4 apart from the other compositions. With an efficiency of 78%, x=4 demonstrates its potential as a high-performance material for energy storage applications. The energy storage characteristics are summarized in Table 1. The energy storage parameters, including maximum polarization, charge energy density (W_{ch}), recoverable energy density (W_r), and efficiency, exhibit distinct differences across the samples. For x=0, the maximum polarization reached 16.85 Cm^{-2}, but its recoverable energy remained low, resulting in an efficiency of just 28%. In contrast, for x=4, although the maximum polarization slightly decreased to 16.62 Cm^{-2}, both the recoverable energy and efficiency saw a significant boost, with recoverable energy increasing to 1.10 J/cm³ and efficiency rising to an impressive value of 78%.

5. Conclusion

The synthesis of $BaTiO_3$- Nb_2O_5 powders was magnificently carried out using the solid-state route. XRD analysis confirmed the absence of any reaction products other than Nb and $BaTiO_3$. The $BaTiO_3$ phase was cubic at room temperature and for compositions with 2% Nb_2O_5 and above, the merging of split peaks indicated the formation of a pseudo-cubic phase. The SEM images indicate that the x=2% composition possesses a porous microstructure with grains larger than 1 nm, while the x=4% composition displays a more compact structure and a finer average grain size of less than 1 nm. The heat treatment significantly improved the dielectric properties of the composite powder. With the increase in Nb_2O_5 concentration, there was a notable rise in the dielectric permittivity, while the dielectric loss showed a modest increase. The findings of this study demonstrate that incorporating Nb_2O_5 significantly enhances the material's dielectric and energy storage properties, with a high dielectric constant of 2200 at 4%, along with an

energy density of 1.40 J/cm^3, a recoverable energy density of 1.10 J/cm^3, and an efficiency of 78.8%. These exceptional properties indicate potential of the optimal composition (x=4) for energy storage applications.

Authors contribution

Abdur Rehman Qureshi and Muhammad Jamshed conceptualized the study, supervised the research, and contributed to the design of the methodology and manuscript revisions. Zama Jan, Arif Ullah, Uzair Khan, Aftab Majeed and Naimat Ullah Khan participated in data collection, data analysis, and drafting the manuscript. All authors reviewed and approved the final version of the manuscript. Muhammad Jamshed served as corresponding author and ensured the overall quality and completion of the work.

Conflicts of Interest

The authors declare no conflict of interest.

Acknowledgment

The authors are thankful to the Department of Physics, Hazara University, Mansehra-21300, Khyber Pakhtunkhwa, Pakistan, for financial support.

Data Availability statement

The data presented in this study are available on request from the corresponding authors.

Funding: Not applicable (N/A).

REFERENCES

1. Jain, A., A.K. Panwar, and A. Jha, Influence of milling duration on microstructural, electrical, ferroelectric and piezoelectric properties of Ba0. 9Sr0. 1Zr0. 04Ti0. 96O3 ceramic. Ceramics International, 2016. 42(16): p. 18771-18778.
2. Schulze-Makuch, D., Life in the Universe, Springer. (2018).
3. Wang, D., et al., BiFeO3-BaTiO3: a new generation of lead-free electroceramics. Journal of advanced dielectrics, 2018. 8(06): p. 1830004.
4. Kamani, D. and M. Ardehali, Long-term forecast of electrical energy consumption with considerations for solar and wind energy sources. Energy, 2023. 268: p. 126617.
5. Dincer, I., Renewable energy and sustainable development: a crucial review. Renewable and sustainable energy reviews, 2000. 4(2): p. 157-175.
6. Sadeghi, G., Energy storage on demand: Thermal energy storage development, materials, design, and integration challenges. Energy Storage Materials, 2022. 46: p. 192-222.
7. Suberu, M.Y., M.W. Mustafa, and N. Bashir, Energy storage systems for renewable energy power sector integration and mitigation of intermittency. Renewable and Sustainable Energy Reviews, 2014. 35: p. 499-514.
8. Chao, S., Ceramic dielectrics for high energy density capacitor application, Missouri University of Science and Technology. (2010).
9. Zhu, Z., et al., Rechargeable batteries for grid scale energy storage. Chemical Reviews, 2022. 122(22): p. 16610-16751.
10. Pan, Z., et al., Achieving high discharge energy density and efficiency with NBT-based ceramics for application in capacitors. Journal of Materials Chemistry C, 2019. 7(14): p. 4072-4078.
11. Powers, R.A., Advances and trends in primary and small secondary batteries. IEEE Aerospace and Electronic Systems Magazine, 1994. 9(4): p. 32-36.
12. Bernard, P. and M. Lippert, Nickel–cadmium and nickel–metal hydride battery energy storage, in Electrochemical energy storage for renewable sources and grid balancing. 2015, Elsevier. p. 223-251.
13. 13. Kaushik, S., et al., Recent advancements in cathode materials for high-performance Li-ion batteries: Progress and prospects. Journal of Energy Storage, 2024. 97: p. 112818.
14. Niu, H., et al., Strategies toward the development of high-energy-density lithium batteries. Journal of Energy Storage, 2024. 88: p. 111666.

15. Randall, C.A., et al. High temperature and high energy density dielectric materials, IEEE Pulsed Power Conference. (2009).
16. Li, D., et al., PE hysteresis loop going slim in Ba 0.3 Sr 0.7 TiO 3-modified Bi 0.5 Na 0.5 TiO 3 ceramics for energy storage applications. Journal of Advanced Ceramics, 2020. 9: p. 183-192.
17. Li, Q., et al., High-temperature dielectric materials for electrical energy storage. Annual Review of Materials Research, 2018. 48(1): p. 219-243.
18. Yao, Z., et al., Homogeneous / inhomogeneous - structured dielectrics and their energy-storage performances. Advanced Materials, 2017. 29(20): p. 1601727.
19. Laghari, J.R. and W.J. Sarjeant, Energy-storage pulsed-power capacitor technology. IEEE transactions on power electronics, 1992. 7(1): p. 251-257.
20. Garcia, C.A.T., Materials Characterization for Sub-micron Superconducting Interconnects in Reciprocal Quantum Logic Circuits, University of Maryland, College Park. (2022).
21. Liu, C., et al., Advanced materials for energy storage. Advanced materials, 2010. 22(8): p. E28-E62.
22. Şahin, M.E., F. Blaabjerg, and A. Sangwongwanich, A comprehensive review on supercapacitor applications and developments. Energies, 2022. 15(3): p. 674.
23. Kerrigan, R. New polymer film type capacitor for high frequency high voltage applications, 44th Electronic Components and Technology Conference, IEEE. (1994).
24. Chu, B., et al., A dielectric polymer with high electric energy density and fast discharge speed. Science, 2006. 313(5785): p. 334-336.
25. Pal, V., R. Dwivedi, and O. Thakur, Dielectric and Ferroelectric Properties of Lead-Free [1-z {(Bi 1-x La x) 0.5 (Na 1-y Li y) 0.5 TiO 3}-z BaTiO 3] Ceramic System. Advances in Materials Science and Engineering, 2013. 2013(1): p. 125634.

How to cite this article:
Qureshi A.R., Jan Z., Ullah A., Khan N.U., Khan U., Majeed A., Jamshed M. (2024). Fabrication and Analysis of $BaTiO_3$-Nb_2O_5 Ceramics for Advanced Energy Storage Applications. *Journal of Chemistry and Environment.* 4(1). p. 18-26.